



A combination of surface-initiated controlled radical polymerization (SET-LRP) and click-chemistry for the chemical modification and fluorescent labeling of cellulose nanofibrils: STED super-resolution imaging of a single fibril and a single fibril embedded in a composite

Xuehe Jiang · J. Benedikt Mietner ·
Julien R. G. Navarro

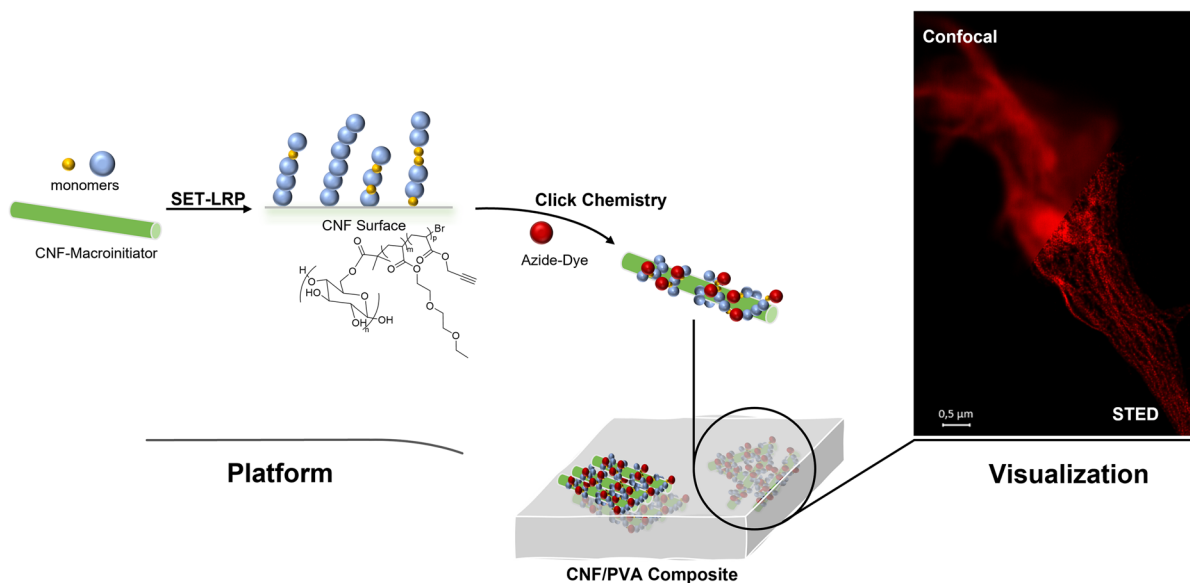
Received: 1 July 2022 / Accepted: 1 December 2022 / Published online: 21 January 2023
© The Author(s) 2023

Abstract A strategy is developed to modify cellulose nanofibril (CNF) surfaces with a combination of Cu⁰-mediated radical polymerization (SET-LRP) and Cu^I-catalyzed azide-alkyne click-chemistry (CuAAC). CNFs were grafted with statistical copolymers of di(ethylene glycol) ethyl ether acrylate (DEGEEA) and acrylic acid 3-trimethylsilyl-prop-2-ynyl ester (TMSPgA) that allows labeling of multiple fluorescent dyes, e.g. AF488 and ATTO633,

special dyes for confocal laser scanning microscopy and stimulated emission depletion (STED) microscopy. Through our strategy and these microscopic techniques, we visualized isolated fibrils and fibrils embedded in a PVA composite in a high resolution. This work also provides new insight into the effect of the clickable entity/precursor on the compatibility of modified fibrils with the composite matrix.

X. Jiang · J. B. Mietner · J. R. G. Navarro (✉)
Institute of Wood Science, Universität Hamburg,
Hamburg, Germany
e-mail: Julien.navarro@uni-hamburg.de

Graphical abstract



Keywords Cellulose nanofibrils (CNFs) · Single electron transfer living radical polymerization (SET-LRP) · Grafting-from · Azide-alkyne click chemistry · STED · Bio-based nanocomposite

Abbreviations

CNFs	Cellulose nanofibrils
SET-LRP	Single electron transfer living radical polymerization
CuAAC	Cu(I)-catalyzed azide-alkyne cycloaddition
STED	Stimulated emission depletion microscopy
PVA	Poly(vinyl alcohol)
DEGEEA	Di(ethylene glycol) ethyl ether acrylate
Me6-TREN	Tris[2-(dimethylamino)ethyl]amine
CDI	1,1'-Carbonyldiimidazole
TEA	Triethylamine
DMSO	Dimethyl sulfoxide
NaASC	L-ascorbic acid sodium salt
TBAF	Tetrabutylammonium fluoride
TMSPgA	Acrylic acid 3-trimethylsilyl-prop-2-ynyl Ester

Introduction

Nowadays, oil-based materials and resultantly plastic waste and plasticizers have become a significant concern for our planet. Therefore, there is a constantly increasing interest in minimizing the environmental impact of those oil-based products. More and more attention has been given to the utilization of ligno-cellulosic biomass for developing a more sustainable human society. Cellulose is a biodegradable, recyclable, renewable polymer and has already found great interest in numerous fields and potential new applications ranging from a flexible gas sensor, water purification to tissue engineering and drug delivery (Ottenhall et al. 2017; Poonguzhali et al. 2018; Hur et al. 2022).

Cellulose nanofibrils or cellulose nanofibers (CNFs), one of the few nanostructured forms of cellulose, can be assimilated to high aspect ratio wires with an average width of 5–60 nm and several micrometers in length (Klemm et al. 2011). The accurate measurement of the fibril length remains a difficult challenge due to their curved morphologies and

the fibril aggregation behavior. CNFs are generally prepared by pre-treatment and delamination of cellulosic materials through mechanical disintegration (Kalia et al. 2014). CNFs have an abundant number of hydroxy, leading to some drawbacks such as hygroscopic character, instability in many organic solvents, strong inter-fibril hydrogen interactions (leading to fibril aggregation) which ones can drastically limit the use of the CNFs in numerous applications. To avoid those undesirable CNF behaviors, CNFs must be subjected to a surface modification process.

Common chemical surface modification of CNFs includes reactions of hydroxy with small molecules through silylation, (Xhanari et al. 2011) acetylation, (Nogi et al. 2006; Gustavsson et al. 2020) esterification, (Lee et al. 2014; Willberg-Keyriläinen et al. 2017), oxidation, (Liimatainen et al. 2012; Fukuzumi et al. 2014; Zhang and Liu 2018) and click-chemistry (Junka et al. 2014; Hettegger et al. 2016; Beaumont et al. 2018; Aïssa et al. 2019). However, through those mentioned reactions, the substitution degree remains low, limiting the suspendability of the CNFs in numerous organic solvents. Another chemical surface modification approach is the grafting of polymers. Polymerization is an optimal strategy to alter the CNF characteristics and properties as polymerization grows long molecular chains on the CNF backbone, creating, for example, optimal interphase between the CNFs and the surrounding medium such as solvent, host matrix (e.g. polymer) and therefore increasing the CNF stability and processability (e.g. composite production).

Grafting polymerizations can be achieved via three main approaches: “grafting to”, “grafting from”, and “grafting through” (Lizundia et al. 2016). The “grafting to” approach covalently attaches existing, pre-formed polymers onto cellulose surfaces (Tsubokawa et al. 2000). The “grafting from”, also known as surface-initiated polymerization (SIP), involves the immobilization of reactive moieties onto a surface, which therefore initiates the propagation of a monomer. Examples of “grafting from” reactions involve Ring-Opening Polymerization (ROP), (Wang et al. 2007; Lalanne-Tisné et al. 2020) as well as controlled or Living Radical Polymerization (LRP) techniques, (Rosen and Percec 2009) such as Reversible Addition-Fragmentation chain Transfer (RAFT), (Chiefari et al. 1998) Atom Transfer Radical Polymerization (ATRP), (Chiefari et al. 1998) and Single-Electron

Transfer Living Radical Polymerization (SET-LRP) (Zhang et al. 2014a). The “grafting through” strategy can be considered as an intermediate approach between the two strategies described above (Kelly et al. 2021).

Cu⁰-mediated SET-LRP, first introduced by Percec et al. (2006) was described as the “ultrafast synthesis of ultrahigh molecular weight polymers”. The reaction can be performed in the presence of oxygen, non-inert condition, or even in the presence of water while keeping control of the polymer molecular weight (Nguyen et al. 2010, 2012, 2013; Fleischmann and Percec 2010; Nicol et al. 2012; Levere et al. 2013; Samanta et al. 2015). SET-LRP proved to be effective with a large library of hydrophilic or hydrophobic vinyl monomers on CNFs (Majoinen et al. 2011; Samanta et al. 2013; Larsson et al. 2013; Navarro et al. 2020).

“Click Chemistry” is a term describing modular reaction, while offering high yield and in-offensive by-products (Wang et al. 2003). It requires simple synthetic conditions, easy removal of the solvents and simple product isolation. Few reactions already meet these criteria, such as the Diels–Alder cycloaddition (Inglis et al. 2009; Kloetzel 2011) or the thiol–ene reaction (Nilsson et al. 2008; Xiong et al. 2018). In addition, the Cu^I-catalyzed azide-alkyne cycloaddition (CuAAC) can also be classified as a click chemistry reaction. One noticeable fact is that biomolecules can preserve their bioactivity within this simple, efficient reaction, which contributes to the vast array of biomedical applications of click chemistry (Himo et al. 2005; Hein and Fokin 2010; Presolski et al. 2011; Song et al. 2012; Kaur et al. 2021). As its popularity increased over the year, a large library of starting compounds is available, making this reaction very attractive to the scientific community (Akeroyd and Klumperman 2011; Ramapanicker and Chauhan 2016).

The interest in using CNFs as fillers or reinforcing agents in bio-based composites is constantly increasing as CNFs offer many advantages, such as relatively low-cost, it can be extracted from numerous renewable resources, meaning a high abundance and availability all over our planet and high mechanical properties (Moon et al. 2011). Over the last few years many research groups devoted their research interest to wood flour, cellulose fiber or cellulose nanofibrils reinforced composites, aiming to better understand the filler-matrix compatibility, their interaction

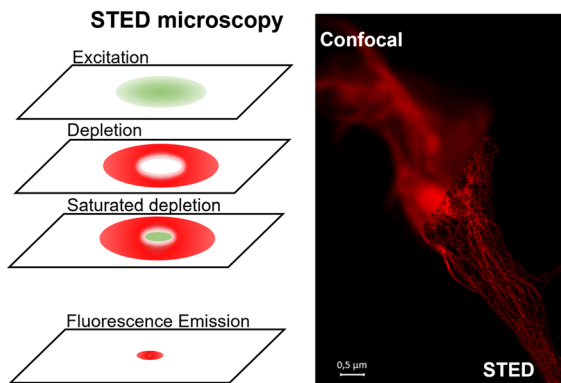


Fig. 1 *Left* Illustration of stimulated emission depletion (STED) Microscopy; (Huang et al. 2010) *Right* comparison of confocal laser scanning microscopy and STED microscopy images of modified cellulose nanofibrils labeled with a fluorescent dye

through their interface and the morphological/dimensional aspect, e.g. homogeneous dispersion and orientation of the filler in the matrix (Saba et al. 2017; Arof et al. 2019; Radakisnin et al. 2020).

The current characterization techniques such as Scanning Electron Microscopy (SEM) or Atomic Force Microscopy (AFM) have been the most widely used tools for imaging and localizing the cellulose fibrils/fiber either alone or in the thermoplastic matrix. Despite the fact that these advanced microscopy techniques have very high resolutions, the elucidation of how CNFs organize themselves when embedded in a polymer matrix remains a challenge, as generally, in composite images, the direct observation of a single buried CNF is significantly harder.

Nakagaito et al. (2004) made detailed scanning electron images of cellulose materials from pulp fiber to CNFs and evaluated the effect of the cellulose morphological changes on the mechanical properties of composites. Fazeli et al. (2018) showed the clear microstructure of individual CNFs with width ranging from 51 to 103 nm via SEM and analyzed the surface roughness of the composite of CNFs reinforced thermoplastic starch via AFM. Frone et al. (2013) discussed CNF dispersion in polylactic acid composites from aspects of the maximum surface height of composites and aggregate sizes of CNFs on the surfaces via advanced AFM. In a bio-based composite material, imaging single cellulose fibrils in the matrix are unfortunately not possible using traditional

microscopy. However, with new technology development such as stimulated emission depletion (STED) microscopy, imaging a luminescent CNF embedded in a polymer matrix could be possible.

Stimulated emission depletion (STED) microscopy is one of super-resolution microscopy techniques that has been developed over decades to overcome the diffraction limit of light microscopy. In STED microscopy, a depletion laser pattern overlaps with the exciting laser and brings excited fluorophores back to the ground state to prevent fluorescence emission in the predefined regions so that it reduces the amount of spontaneous fluorescence emission (Fig. 1) (Huang et al. 2010). As a result, the effective point spread function is lower than the diffraction limit, thus achieving a high resolution down to 20 nm (Vicidomini et al. 2018). STED microscopy has been a versatile tool for biological research (Roo-bala et al. 2018; Stephan et al. 2019; Sezgin et al. 2019) and nanoscale materials (Friedemann et al. 2011; Busko et al. 2012; Liu et al. 2021) as it allows living-cell imaging, (Stockhammer and Bottanelli 2021; Calovi et al. 2021) 3D imaging as well as fast imaging, (Schermelleh et al. 2010) and there is a wide range of commercially available fluorophores suitable for it. Another specialty of STED is deep imaging, by reducing specimen-induced spherical aberration, STED microscopy achieved a resolution of 60–80 nm, 120 μm deep inside scattering biological tissue (Urban et al. 2011). However, to characterize CNFs with STED microscopy, a specific luminescent dye has to be labeled onto the CNFs.

The labeling of cellulose nanomaterials with fluorescent dyes is of interest in biomedical and sensor applications (Edwards et al. 2013; Guise and Fanguero 2016; Golmohammadi et al. 2017; Wu et al. 2018; Zhai et al. 2022). Fluorescently tagged CNFs are also used for the study of, for instance, nanotoxicology and therapeutics. (Salari et al. 2019; Ning et al. 2021) Schyrr et al. (2014) prepared CNF/PVA nanocomposites with a high concentration of fluorescent sensor motifs by thiol-ene click reactions. Navarro et al. (2015) modified CNFs with furan and maleimide groups to enable selective labeling of fluorescent probes through Diels–Alder cycloaddition and thiol-ene click reaction. Goodge et al. (2020) functionalized biotin-CNF membranes with the substitution of alkyne groups, and fluorescently tagged azide-biotin

conjugate via copper-catalyzed alkyne-azide cycloaddition (CuAAC). Recently, a fluorescence-labeling approach on CNFs via a triazine linker and click-chemistry is also reported (Babi et al. 2022). In all these studies, the labeling of CNFs was achieved through specific chemical reactions sequentially inducing certain precursors, followed by one or two click-chemistry reactions.

Our aim, in this paper was to develop a multifunctional platform made of a bio-based polymer nanostructure, the cellulose nanofibrils, that could be easily tunable to adapt to numerous and various applications. To prove our concept idea, we focus this study on labeling the CNFs with specific luminescent dyes and performing single-molecule imaging of isolated fibrils and fibrils embedded in a composite.

We develop a strategy to surface modify the CNFs through Cu⁰-mediated radical polymerization and finally introduce different luminescent dyes via post-modification through Cu^I-catalyzed azide-alkyne click-chemistry. For this purpose, after synthesizing the CNF-based macroinitiators, statistical copolymers were grafted onto the CNFs through Surface Initiated SET-LRP. The monomers comprise a di (ethylene glycol) ethyl ether acrylate (DEGEEA) and a protected alkyne monomer (Acrylic Acid 3-trimethylsilyl-prop-2-ynyl Ester, TMSPgA). DEGEEA was employed to increase the stability of the CNFs in selected solvent (DMSO & H₂O), while it is well known that hydrogen bonding enhanced the inter-fibril interaction yielding aggregation of fibrils automatically. So, this monomer aims to suppress this issue but also to act as a spacer between neighbor luminescent dyes by spacing the reactive clickable monomers. TMSPgA was used to introduce the reactive luminescent dyes on the CNF surface. Unfortunately, this alkyne monomer needed to be protected during the polymerization reaction and later-on deprotected. SET-LRP could not be performed without this protection step. Finally, the morphology of the modified CNFs was investigated through confocal laser scanning microscopy and stimulated emission depletion (STED) microscopy. Within the STED microscopy technique, we could visualize isolated fibrils and fibrils embedded in a composite. Moreover, we could also tune the compatibility of the modified CNFs within the matrix, by simply changing the clickable entity/precursor, and therefore change drastically the adhesion of the CNFs within the composite matrix. Those changes, which could not be observed with traditional electron

microscopy techniques (SEM, AFM), were possible with the STED.

Experimental section

Materials

1,1'-carbonyldiimidazole (CDI, 98%), 3-(Trimethylsilyl)propargyl alcohol (98%) were purchased from abcr. Dimethyl sulfoxide (DMSO, ≥99%), imidazole (≥99%), anhydrous diethyl ether (99%), acryloyl chloride (96%), tris[2-(dimethylamino)ethyl]amine (Me₆-TREN, 98%), copper(II) sulfate pentahydrate (CuSO₄·5H₂O, ≥99%), L-ascorbic acid sodium salt (NaASC, 99%), poly(vinyl alcohol) (PVA, 98–99%), Cu wire (diameter 0.812 mm, 99.9%) were purchased from Alfa Aesar. 2-bromo-2-methylpropionic acid (98%), di(ethylene glycol) ethyl ether acrylate (DEGEEA, 90%), hydroquinone (99%), triethylamine (TEA, 99%), sodium carbonate (Na₂CO₃, 99.5%), hydrogen chloride solution (0.1 M), tetrahydrofuran (THF, 99.9%) and azide fluor 488 (AF488, ≥90%) were purchased from Sigma-Aldrich. Acetone (99.90%) was purchased from BCD-Chemie. Acetic acid (AcOH, 99%) was purchased from Chemsolute. Ethyl 2-bromo-2-methyl propionate (EBiB, 98%) was purchased from Fisher. Tetrabutylammonium fluoride (TBAF, 1 M in THF) and 3-azido-7-hydroxyl-coumarin were purchased from TCI Chemical. ATTO633 was purchased from ATTO-TEC GmbH.

To produce cellulose nanofibrils (CNFs), dried elemental chlorine-free (ECF) bleached kraft pulp (Stendal GmbH, Germany) was used, and the CNF suspension was obtained with the use of a Microfluidizer (M-110EH-30 Microfluidics, Indexcorp).

DI water (0.055 μS/cm) was used for the solvent-exchange procedure and synthesis.

All the monomers for grafting polymerization were passed through a basic alumina column to remove inhibitors.

Production of cellulose nanofibrils

Cellulose nanofibrils were produced as previously described (Mietner et al. 2021). In a general procedure, cellulose pulp suspended in water was firstly ground to 75–80°SR (SR: Schopper-Riegler degrees), then passed through chambers with orifice widths of

400 μm and 200 μm (2 times), 200 μm and 100 μm (4 times) successively under high pressure. The process resulted in a 2% (w/w) CNF aqueous gel. The CNF gel was refrigerated at 5 $^{\circ}\text{C}$.

Solvent exchange procedure

The solvent exchange procedure of the CNF aqueous gel proceeded as previously described (Navarro and Edlund 2017). In general, DMSO was slowly added to the aqueous suspension of CNFs under stirring. Then, the solvent was discarded by centrifugation and replaced with fresh DMSO. The procedure resulted in a 2% (w/w) CNF/DMSO gel.

Synthesis of the CNF-based macroinitiator (CNF-MI)

CNF-based macroinitiator was produced as previously described (Georgouvelas et al. 2020). The suspension of CNFs in DMSO was added with imidazole and degassed via nitrogen purging continuously. Separately, a solution of 2-bromo-2-methyl propionic acid in DMSO was prepared and purged with nitrogen for 10 min; then CDI was slowly added under stirring at room temperature until it was fully dissolved, and no gases were further produced. Finally, the solution was slowly added to the CNF suspension. The reaction proceeded under a nitrogen atmosphere overnight at 55 $^{\circ}\text{C}$. The modified CNFs were purified by sequential washing with DMSO (4 \times 30 ml), centrifugation (4427 rcf for 30 min), and decantation. The process resulted in a 1% (w/w) CNF-MI gel.

Synthesis of acrylic acid 3-trimethylsilyl-prop-2-ynyl ester (TMSPgA)

3-(Trimethylsilyl) propargyl alcohol (5 g, 39 mmol), TEA (7.61 mL, 54.6 mmol), and hydroquinone (30 mg, 0.3 mmol) were dissolved in anhydrous diethyl ether (50 mL) and cooled in an ice–water bath. A solution of acryloyl chloride (3.80 ml) in diethyl ether (20 mL) was added dropwise over 30 min. The reaction was set up in an inert atmosphere under nitrogen; the mixture was stirred in the ice bath for 1 h and then at ambient temperature overnight. The final product was obtained by extraction with Na_2CO_3 solution (1 M aq., 3 \times 100 mL) and rotary evaporation of the collected organic phase.

Synthesis of statistical copolymer of DEGEEA and TMSPgA onto CNFs (DEG-TMSPgA-CNF) via SET-LRP

The copolymerization of statistical copolymer DEG-TMSPgA-CNF (DEGEEA:TMSPgA = 6:4) was carried out in one pot. DEGEEA (9.24 mmol) and TMSPgA (6.16 mmol) in DMSO (15 ml) were added into a suspension of CNF-MI (4 g, 1% w/w) in DMSO (30 mL). Separately, a Cu wire (diameter = 0.812 mm, length = 6 cm) was immersed in a concentrated HCl solution for 10 min, then rinsed with water and acetone and dried prior to use. The suspension with Cu-wire was degassed via nitrogen purging for 10 min and raised to 40 $^{\circ}\text{C}$. The reaction started when the Me6-TREN ligand (200 μL , 10% v/v in DMSO) was added and proceeded overnight under a nitrogen atmosphere. The modified CNFs were purified by sequential washing with DMSO (6 \times 30 ml), centrifugation (4427 rcf for 30 min), and decantation.

Syntheses of statistical polymer DEGEEA and TMSPgA (DEG-TMSPgA, DEGEEA:PgA = 6:4) was also carried out according to the description above, except that the ethyl 2-bromo-2-methyl propionate (EBiB) replaced the CNF-MI as a sacrificial initiator at a $[\text{M}]_0/[\text{I}]_0/[\text{L}]_0$ ratio of 100/1/0.2.

Deprotection of trimethyl silyl (TMS) protected polymers

The TMS-protected polymer (TMSPgA induced CNFs, DEG-TMSPgA-CNF 2.9 g, 6.16 mmol TMS groups in theory) was suspended in THF (72 ml) with the addition of acetic acid (0.7 ml, 2 equiv. mol/mol to TMS groups). The suspension was purged with nitrogen and cooled to -20°C . A 1 M solution of TBAF \cdot 3 H_2O in THF (2 equiv. mol/mol to the TMS groups) was slowly added. The mixture was stirred at -20°C for 30 min and then warmed to ambient temperature overnight. The deprotected polymer was purified by sequential washing with THF (4 \times 50 ml), centrifugation (4427 rcf for 30 min), and decantation.

General procedure of CuAAC click reaction

A suspension of an alkyne-containing polymer (TMS-deprotected CNFs, DEG-PgA-CNF 4 mg (dry), 10 μmol alkyne groups in theory) in DMSO (1.6 ml), and a solution of 3-azido-7-hydroxyl-coumarin in

DMSO (5 mM, 2 equiv. mol/mol to alkyne groups) was mixed under an inert atmosphere of nitrogen. Separately, a solution of CuSO_4 (20 M aq., 0.15 equiv. mol/mol to alkyne groups) and sodium ascorbate (100 mM aq., 3 equiv. mol/mol to alkyne groups) in H_2O was deoxygenated and then transferred in the suspension. The resulting suspension was covered by aluminum foil and stirred under nitrogen at room temperature for 24 h. The product was purified by sequential washing with DMSO (4×5 ml), centrifugation (4427 rcf for 30 min), and decantation.

The same procedure was performed for labeling DEG-PgA-CNFs with fluorescent dyes AF 488 and ATTO 633, respectively, except 0.5 mg azide dye was used for 1 g DEG-PgA-CNFs (1% w/w).

Blending of PVA with modified CNFs

Two concentrations of PVA/DMSO solution were prepared: 5–10%. PVA was dissolved in DMSO at 80 °C with constant stirring and cooled down to room temperature. The suspension of modified CNFs with different dyes in DMSO was fully blended into each PVA/DMSO solution, respectively, resulting in the final concentration of all modified CNFs at 0.5% w/w.

Characterization

Fourier transform infrared spectroscopy equipped with an attenuated total reflection (ATR-FTIR) was performed using a Bruker Vector 33 spectrometer. All spectra were obtained as means of 60 scans in the spectral region of 3600–550 cm^{-1} , with a spectral resolution of 4 cm^{-1} .

Ultraviolet–visible (UV–Vis) spectroscopy was carried out with a Lambda 65 UV–vis Spectrometer. Absorption spectra were measured in DMSO from 380 to 900 nm with a resolution of 1 nm in a 10 mm quartz cuvette.

Proton nuclear magnetic resonance (^1H -NMR) experiments were performed on a Bruker Avance-III spectrometer HD 400 MHz operating at 400 MHz at room temperature. Samples were dissolved in chloroform- d and transferred to NMR tubes.

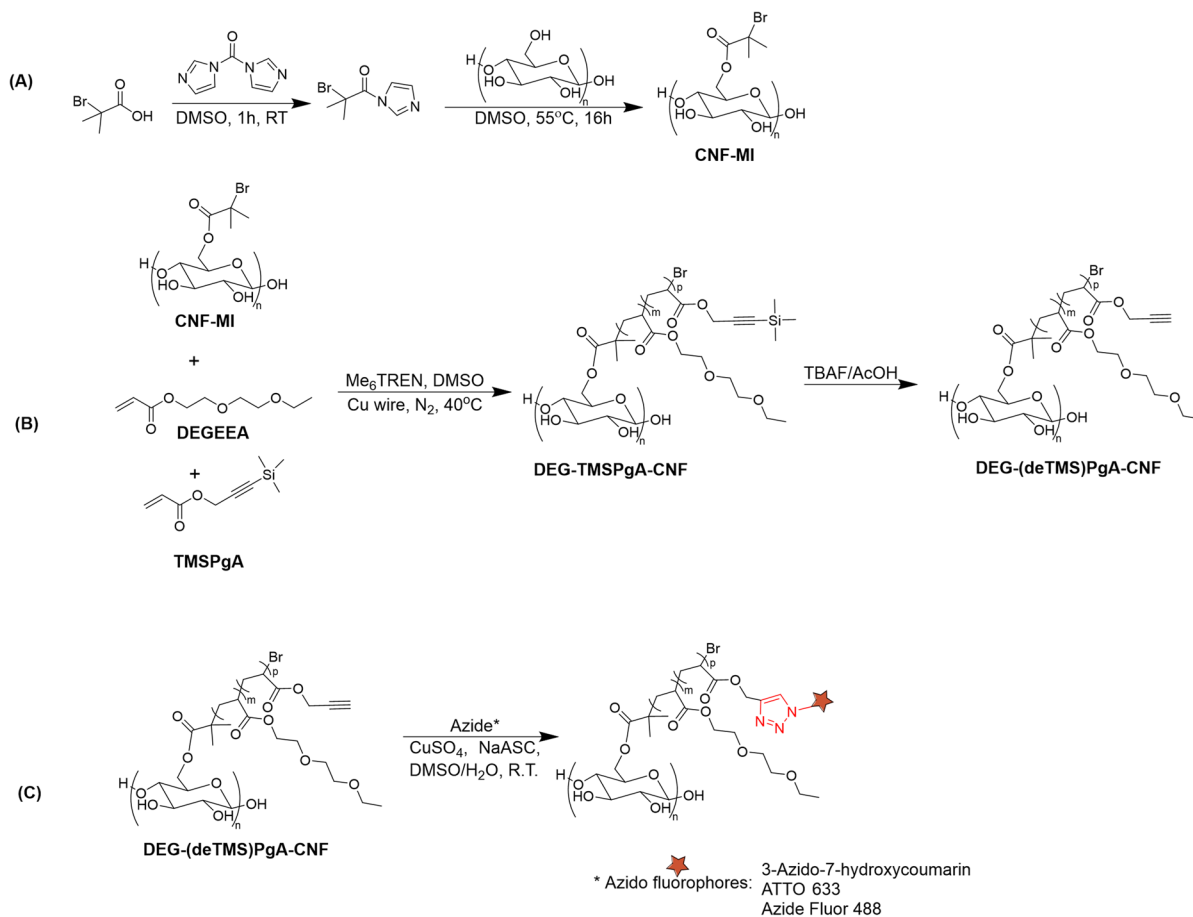
All ^{13}C NMR spectra were acquired with a Bruker 500 Avance III HD spectrometer at Larmor frequencies of 125–500 MHz for ^{13}C and ^1H , respectively.

The samples were packed in 4 mm zirconia rotors to carry out magic angle spinning (MAS) with a spinning rate of 8 kHz. Ramped cross-polarization (CP) ^{13}C MAS NMR spectra were recorded with a ^{13}C nutation frequency of 10 kHz and a contact time of 1.5 ms. All spectra were obtained by Fourier transform of the FIDs, and the chemical shifts were quoted relative to neat tetramethylsilane (TMS).

The morphology of modified CNFs in PVA was observed via ultra-high-resolution field emission scanning electron microscopy (FE-SEM) of the Hitachi S-800. The dried samples were mounted on sample supports using carbon tape and coated with a 5 nm layer of Pd/Pt with a Cressington 208HR under an inert atmosphere.

Stimulated Emission Depletion Microscopy (STED) super-resolution imaging were performed on 1.5H fixed coverslips using a STEDYCON scanner with 488, 561 and 640 nm excitation lasers together with a 775 nm STED laser (all pulsed) (Abberior Instruments GmbH, Göttingen, Germany). The STEDYCON was attached to a Zeiss Axio-imager Z2 with a 100×/1.46 NA oil immersion Apochromat objective. Depletion power was set to achieve a resolution of 40 nm, the pinhole was set at 50 μm , and the sampling rate was fixed at 20 nm/px. The samples were dried on cover glasses under vacuum and mounted on slide glasses with Abberior MOUNT embedding media.

Deconvolution and post-process were used by software Huygens Essential and Zeiss Zen. We used iterative CMLE (Classical Likelihood Estimation) deconvolution with a maximum of 30 iterations to prevent over-deconvolution using the Huygens Professional software package. This algorithm has been validated multiple times and is considered standard in deconvolution. The software package includes a module to estimate the point spread function (PSF) specifically for STEDYCON scanners fitted with a 1.46 NA lens. Moreover, the theoretical PSF was tuned to match the experimental PSF as closely as possible, providing the software with input regarding pixel size (sampling), refractive index mismatch, depth of imaging, wavelength, projected pinhole radius and STED saturation factor.



Scheme 1 General chemical strategy for the polymer grafting onto the cellulose nanofibril (CNF) surface (a) synthesis of the CNF-based macroinitiator (CNF-MI); b Di(ethylene glycol) Ethyl Ether Acrylate (DEGEEA) and the Protected Alkyne

Groups Acrylate (TMSPgA) grafted onto the CNFs via surface initiated SET-LRP, followed by the sequential deprotection of trimethylsilyl groups; c Cu-catalysed azide-alkyne cycloaddition between alkyne-induced CNFs and azido-fluorophore

Results and discussion

Solvent exchange and chemical surface modification of CNFs

Firstly, the unmodified pristine CNFs, initially suspended in water, were solvent exchanged to DMSO. This exchange procedure is an exothermic process due to the water—DMSO interaction and the hydrogen bonding formation between the CNFs and the DMSO. (Voronova et al. 2006) After this, the pristine CNFs, already suspended in DMSO, were surface modified and converted to the CNF-based macroinitiator (CNF-MI) through an esterification reaction between the hydroxy and the 2-bromo-2-methylpropionic acid

(in DMSO). The immobilization of the initiator onto the CNFs, is a one-step process, which will allow us later to directly grow a polymer via the SET-LRP reaction onto the CNF surface using the macroinitiator unit as an anchoring point on the surface. Through this surface-initiated polymerization, the properties of the CNFs can be fully tuned and optimized. The chemical reaction pathway is shown in Scheme 1a.

The correct and successful surface modification was monitored with ATR-FTIR (Fig. 2) and CP-MAS ^{13}C NMR (Fig. 3) spectroscopy. The unmodified CNF spectra show the characteristic bands of the cellulose, with bands localized at 3320 cm^{-1} (O–H), 2950 and 2895 cm^{-1} (C–H), 1430 cm^{-1} (C–H), and 1161 cm^{-1} (C–O–C). In addition to those characteristic bands,

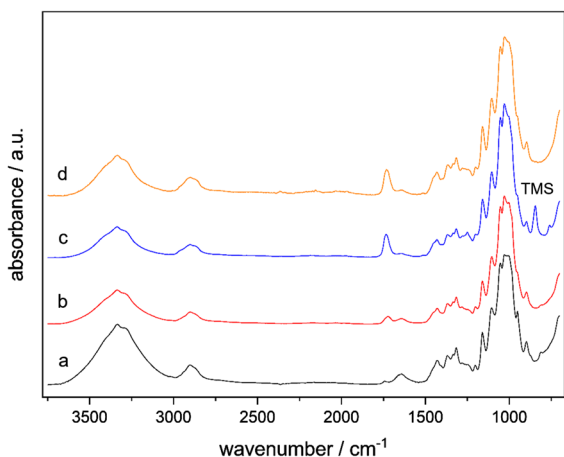


Fig. 2 ATR-FTIR spectra of **a** Pristine CNFs, **b** CNF-MI, **c** DEG-TMSPgA-CNFs and **d** DEG-PgA-CNFs

the spectrum of the CNF-MI shows an absorption band localized at 1733 cm^{-1} ($\text{C}=\text{O}$), which is attributed to the vibration of the carbonyl group of the ester group. The CP-MAS ^{13}C NMR spectra of unmodified CNFs & CNF-MI, along with the peak assignments, are exposed in Fig. 3. The pristine CNFs have the characteristic cellulose NMR peaks located at 105 ppm (C1, glycosidic bonds), 84 ppm (C4), 72 ppm (C2, C3, C5), 62 ppm (C6) for the carbon on surface sites, and at 89 ppm (C4), 76 ppm (C2, C3, C5), 65 ppm (C6) for the crystalline fibril interior (Gårdebjer et al. 2015). Besides the characteristic signals from pristine CNFs, the spectrum of CNF-MI showed an extra peak at 31 ppm (C9, C10). Although the carbonyl signals were not displayed through the solid-state CP-MAS ^{13}C NMR, the successful conversion of CNFs into CNF-MI can be confirmed by combining the results of both ATR-IR and CP-MAS ^{13}C NMR. Within this strategy, chemically modified CNFs can thus act as a macroinitiator, and initiate the polymerization of two different monomers, for the “grafting from” of polymer chains growing directly on the CNF surface.

Surface initiated SET-LRP: growth of the statistical copolymer DEG-PgA-CNF

The surface-initiated grafting polymerization was carried out in a one-step procedure via SET-LRP. The aim was to initiate the growth of statistical copolymers made of di (ethylene glycol) ethyl ether acrylate

(DEGEEA) (Zhang et al. 2014b; Anastasaki et al. 2014; Bao et al. 2018) and a monomer containing alkyne functions in the presence of the CNF-based macroinitiator. The SET-LRP of the two monomers was proceeded in the presence of a Cu(0) wire and a tetradentate tertiary amine ligand (Me_6TREN).

In our first attempt, we tried to initiate the SET-LRP of the unprotected propargyl acrylate. Unfortunately, the CNFs could not be modified within this approach. Some side reactions of alkyne functions took place during Cu-catalyzed radical polymerizations, as the terminal alkyne groups are prone to oxidative coupling (Glaser coupling) in the presence of Cu^1 and oxidants, (Storms-Miller and Pugh 2015) for example, while air exposure during the post-treatment. Therefore, this work employed a protection/deprotection strategy of the alkyne groups. This strategy allowed us to overcome those unwanted side reactions during copolymerization. Firstly, trimethylsilyl propargyl acrylate (TMSPgA) was synthesized through the esterification reaction of acryloyl chloride and 3-(trimethylsilyl) propargyl alcohol; (Malkoch et al. 2005) after the protection step, both monomers TMSPgA and DEGEEA were copolymerized onto the CNF surface (DEG-TMSPgA-CNFs). In the final step, the trimethylsilyl protecting group was removed using a tetra-*n*-butylammonium fluoride (TBAF) solution in THF and acetic acid (AcOH) as the buffering agent to finally yield the deprotected alkyne group, DEG-PgA-CNFs (Scheme 1b).

The efficiency of the co-grafting polymerization of DEGEEA and TMSPgA onto CNFs was first evaluated with ATR-FTIR (Fig. 2c). Compared to the CNF-MI spectra, the carbonyl band at 1733 cm^{-1} in the DEG-TMSPgA-CNFs and DEG-PgA-CNFs spectrum drastically increase due to the multiplication of the ester group number of the polymer repeating unit. The band localized at 1250 cm^{-1} and 700 cm^{-1} are attributed to trimethylsilyl groups (TMS, $\text{Si}(\text{C}-\text{H}_3)$) of the TMS-protected alkynes. This also confirmed that no cleavage of the trimethylsilyl group from the TMS-protected alkynes occurred during and after the surface-initiated polymerization onto CNFs.

After the deprotection step, and the removal of the trimethylsilyl groups from the CNF surface, the absorption bands located at 1250 cm^{-1} and 700 cm^{-1} disappear from the ATR-FTIR spectra, while the signals from carbonyl remain the same. Unfortunately, the alkyne groups on CNFs are more difficult to

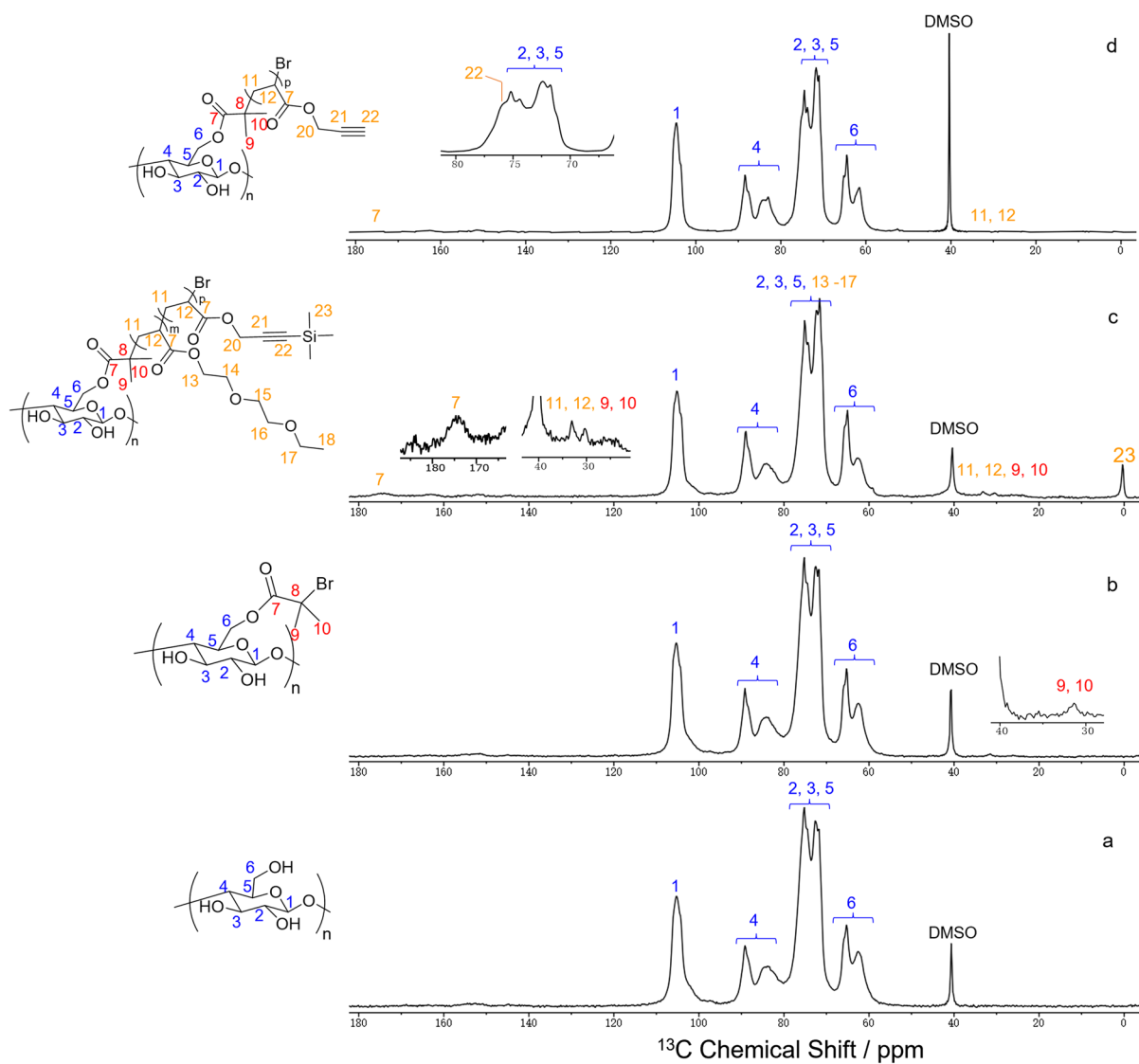


Fig. 3 CP/MAS ^{13}C -NMR spectra of **a** Pristine CNFs, **b** CNF-MI, **c** DEG-TMSPgA-CNF, **d** PgA-CNFs

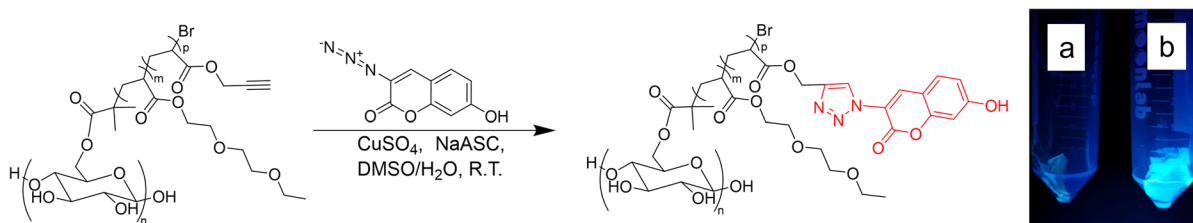


Fig. 4 Click chemistry reaction of DEG-PgA-CNFs and 3-azido-7-hydroxycoumarin: **a** DEG-PgA-CNFs before the reaction, **b** After the reaction with the fluorescence of 3-azido-7-hydroxycoumarin

observe on the spectrum and it remains difficult to distinguish and differentiate them from the background clearly. We further extend the characterization of the product with the solid-state CP-MAS ^{13}C -NMR and the spectra are exposed in Fig. 3. The CP-MAS ^{13}C -NMR results are consistent with the results obtained with the ATR-FTIR. Besides observing, the characteristic CNF peaks, an additional peak located at 175 ppm (C7) appear and is attributed to the carbonyl bonds and the accumulated ester groups of the polymer repeating units. The peak at 0 ppm (C23) is attributed to the trimethylsilyl protecting group. After the deprotection step, besides the disappearance of trimethylsilyl groups, a signal at 76 ppm (C22) is detected from a broad peak overlapped CNFs (C4) and is attributed to the deprotected alkyne groups.

Click chemistry azide-alkyne cycloaddition of alkyne modified CNFs and various fluorescent azides dyes

The proof of the presence of alkyne functions via click chemistry with 3-azido-7-hydroxycoumarin

As mentioned earlier, the surface modification of CNFs through SET-LRP and various monomers was effective; however, the direct presence of the alkyne functions onto CNFs was difficult to observe, and their presence has to be confirmed through the combination

of two characterization techniques. Therefore, to ensure the presence of the alkyne function onto our CNFs, we performed a test click reaction with the DEG-PgA-CNFs and the 3-azido-7-hydroxycoumarin in DMSO/H₂O (Fig. 4). An interesting parameter is the 3-Azido-7-hydroxycoumarin fluorescence properties can only be revealed when the dye reacts with an alkyne function and form 1,2,3-triazole through Cu-catalyzed cycloaddition reactions, otherwise the fluorescence is quenched (Sivakumar et al. 2004). After few minutes, the CNF suspension became highly fluorescent, and after several purification steps, the luminescent CNFs were isolated (Fig. 4).

It should also be stated that this Cu-catalyzed cycloaddition reaction was also performed using unmodified CNFs and CNF-MI (within the same Cu-catalyzed condition). In both cases, the suspensions remained colorless even under UV-light, no reaction occurred since no alkyne function was present (Fig. 4, Picture a). Excessive reagents are unfortunately generally needed to ensure the molecules attachment onto the CNF surface, while the exact amount is still challenging to estimate and even more specifically in our case. In our work, the incorporated reagents for click chemistry were calculated on the free alkyne groups of DEG-PgA-CNFs with 100% chemical conversion of SET-LRP and deprotection (1 μmol alkyne groups in 0.4 mg DEG-PgA-CNFs, dry). 2 equivalents of azide based on alkyne groups were used for

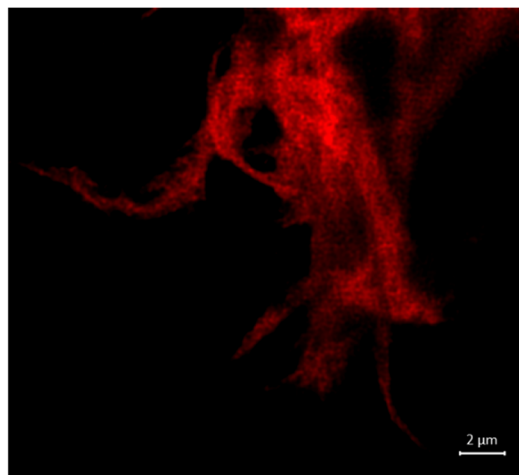
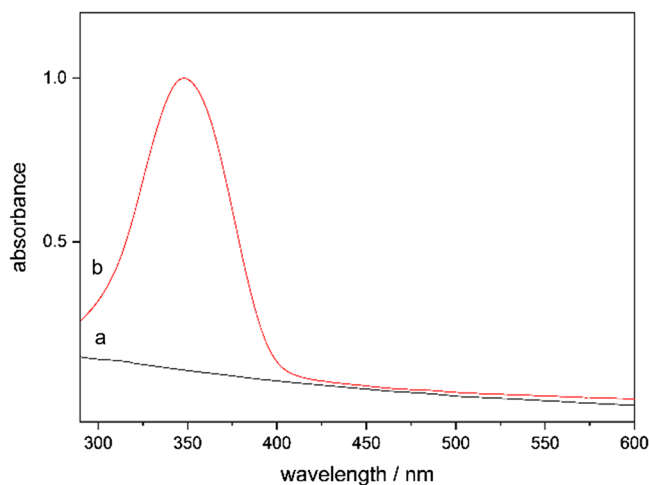
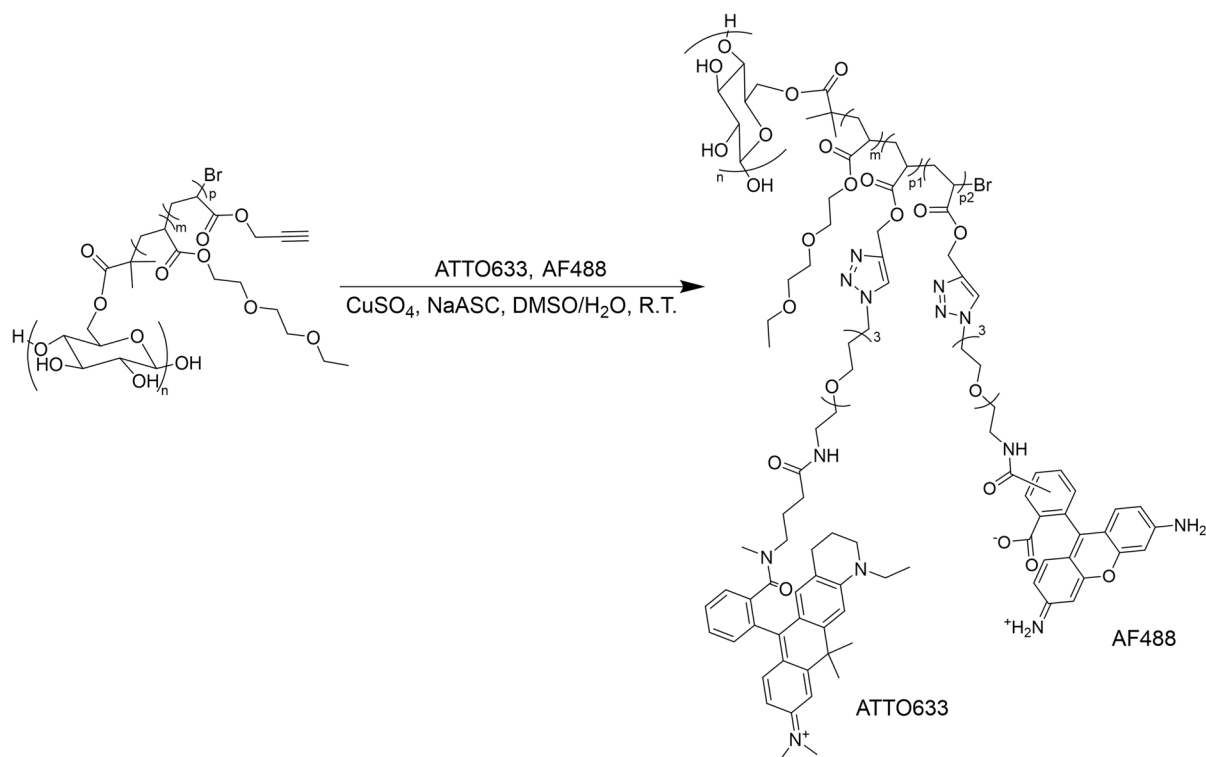


Fig. 5 Left UV-Vis spectra of **a** Pristine CNFs, **b** Coumarin@DEG-PgA-CNFs; Right Confocal scanning laser microscopy imaging of coumarin derivate labelled on the polymer modi-

fied CNFs (Fluorescence image obtained at an excitation wavelength of 488 nm, red color)



Scheme 2 Preparation of the luminescent cellulose nanofibrils: Labeling of the two dyes ATTO633 and AF488 onto the polymer modified CNFs (DEG-PgA-CNF) through click-chemistry

fast reactions and concerning low alkyne contents; the concentration of the Cu catalyst was controlled at $250 \mu\text{M}$ for efficient reactivity. After several purification step, the modified luminescent CNF gel was isolated (Fig. 4, Picture b).

The suspension was first characterized through UV–Vis spectroscopy and the spectra is exposed in Fig. 5. The spectra of the luminescent CNFs show the presence of a strong absorption band at 350 nm , while the spectra of the unmodified CNFs do not show any distinct absorption band. This demonstrates the successful grafting of the coumarin azide dye onto the polymer modified CNFs through a Cu-catalyzed cycloaddition with the alkyne groups (DEG-PgA-CNF). Confocal laser scanning microscopy (CLSM) was used to image the coumarin labeled on the copolymer modified CNFs (Fig. 5, Right). From this CLSM image, it can be seen that fluorescent spots were only observed along the CNFs. Moreover, the fluorescence distribution appears to be homogeneous on the fibril surface.

Click chemistry strategy for STED high-resolution imaging of modified CNFs

As exposed previously, it was possible to label a fluorescent coumarin dye derivative onto the CNFs through a Cu-catalyzed click post-modification reaction. Since the concept worked, our goal was now to label the CNFs with a specific dye and perform STED measurements for single-molecule studies. For this purpose, two dyes the ATTO633 & AF488 were labeled onto the CNFs as exposed in Scheme 2. Both of those dyes have a specific purpose as described in the following.

The AF488 (Abs/Em = $501/525 \text{ nm}$), was initially used to easily localize the CNFs under the microscope. This bright green fluorescent dye is already widely used in confocal microscopy and also has a good spectral separation with the ATTO633. The ATTO633 (Abs/Em = $630/657 \text{ nm}$) fluorescent dye is a red-emitting dye, used especially for the STED microscope due to its photophysical properties, high quantum yield and photo-stability. For

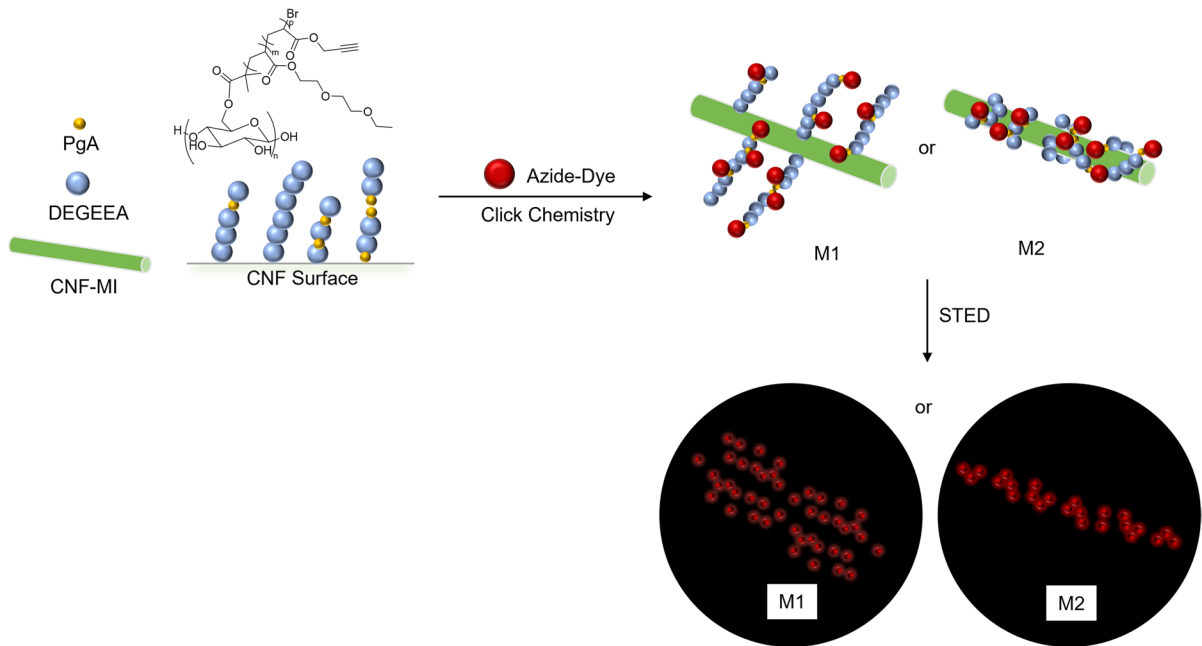
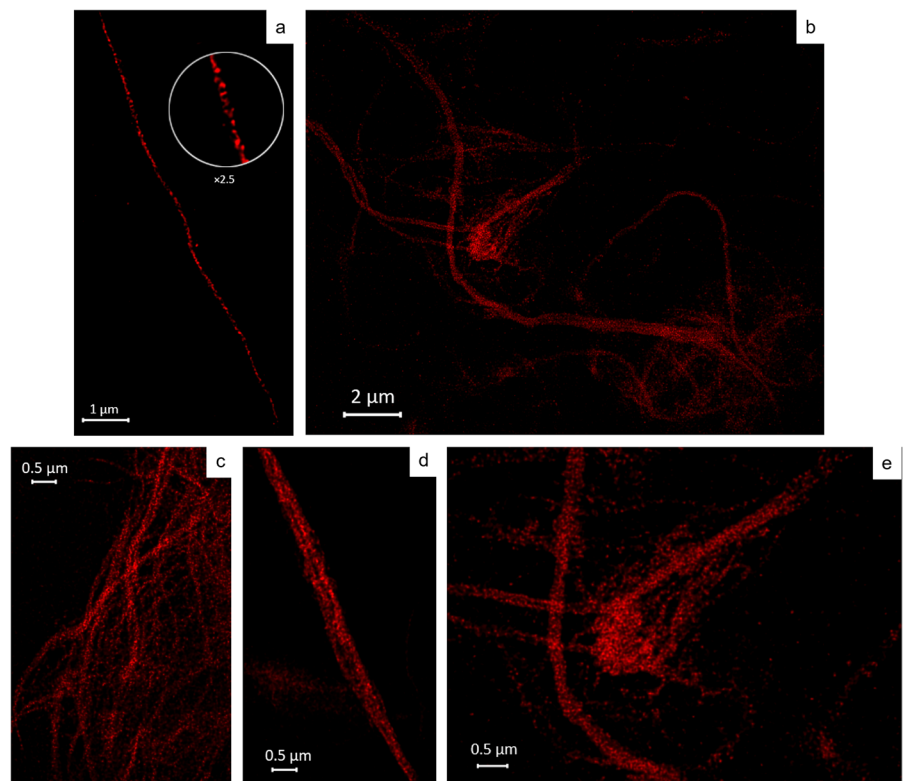


Fig. 6 Schematic illustration of labeling fluorescent dyes on cellulose nanofibril surfaces and hypothetical morphologies of modified CNFs

Fig. 7 Deconvolved STED images of modified cellulose nanofibrils: **a** Isolated fibril, **b** Dispersion state of fibrils, **c** Fibril network, **d** Fibril bundle, **e** Cluster



the purpose of this study, two different batches of fluorescent CNFs were produced, the CNFs labeled with the two dyes AF488 and ATTO633 (AF488&ATTO633@DEG-PgA-CNF) as exposed in scheme 2, and also the CNFs labeled with only the ATTO633 dye (ATTO633@DEG-PgA-CNFs).

As introduced earlier, STED microscopy with the appropriate dyes and the optical scheme can normally achieve a super-high resolution (Fig. 1). For post-processing images, we used deconvolution with a standard algorithm to prevent over-deconvolution, and an experiment specific modelled PSF that was validated measuring 40 nm beads exciting and emitting in the same wavelength ranges as the fibrils.

Therefore, our modified cellulose nanofibrils labeled with special fluorescent dyes as well as in a composite material are ideal objects for investigation with this technique.

STED and high-resolution imaging of modified single CNFs

A suspension of DEG-PgA-CNFs labeled with AF488 and ATTO633 (AF488&ATTO633@DEG-PgA-CNFs) or CNFs only labeled with the ATTO633 (ATTO633@DEG-PgA-CNFs) in DMSO (0.5% w/w) was used for sample preparation to detect isolated modified CNFs and sufficient signals with clean background under the microscope.

We considered hypothetical morphologies of grafted polymer chains stretching away from CNF surfaces (Fig. 6, M1), or wrapping around on CNFs (Fig. 6, M2), which corresponds to fluorescent signals either spreading or wrapping, respectively.

Figure 7 shows a series of deconvolved STED images, in which the fluorophores are represented as red dots and formed into spaghetti-like shapes. For example, in Fig. 7A the fibrils exhibits a fluorescent strip with a width of 56 nm and a length of 9 μm , which match the typical dimension of CNFs produced by mechanical treatments. Interestingly, fluorophores on this strip display a periodical interval (Fig. 7a) with red luminescent dots followed by empty (black) space, which can represent either grafted di(ethylene) glycol chains or unlabeled alkyne function on the CNF surfaces. As mentioned earlier, excess azide dye was employed to ensure the full functionalization of the alkyne groups.

This periodical interval phenomenon was observed among all the CNF images and all our different CNF samples. The study of the morphology of the polymer-modified CNFs revealed that the grafted polymer chains wrap around the CNF surfaces (Fig. 6, M2). In other words, the arrangement of the fluorophores expresses the dimension and morphology of the cellulose nanofibrils and is mostly not influenced by the grafted polymer.

The interactions between several CNF nanostructures were further observed and discussed. Figure 7b provides an overview of the representative CNFs with various inter-fibrillar structures, which could be observed with the STED. The inter-fibrillar nanostructures can be summarized into three types (Fig. 7c–e): homogeneous network, fibril bundle and cluster. The homogeneous network is formed by single fibrils interacting with distances of max. 0.5 μm between them (Fig. 7c); a fibril bundle consists of several aligned fibrils with a thin gap (approx. 50 nm)

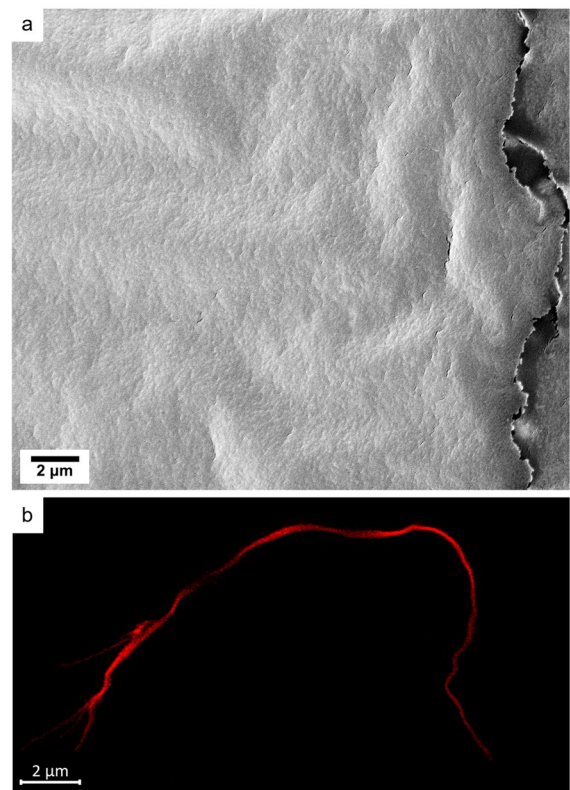


Fig. 8 a FESEM image of Fibrils/PVA composite, b STED image of fibrils in PVA

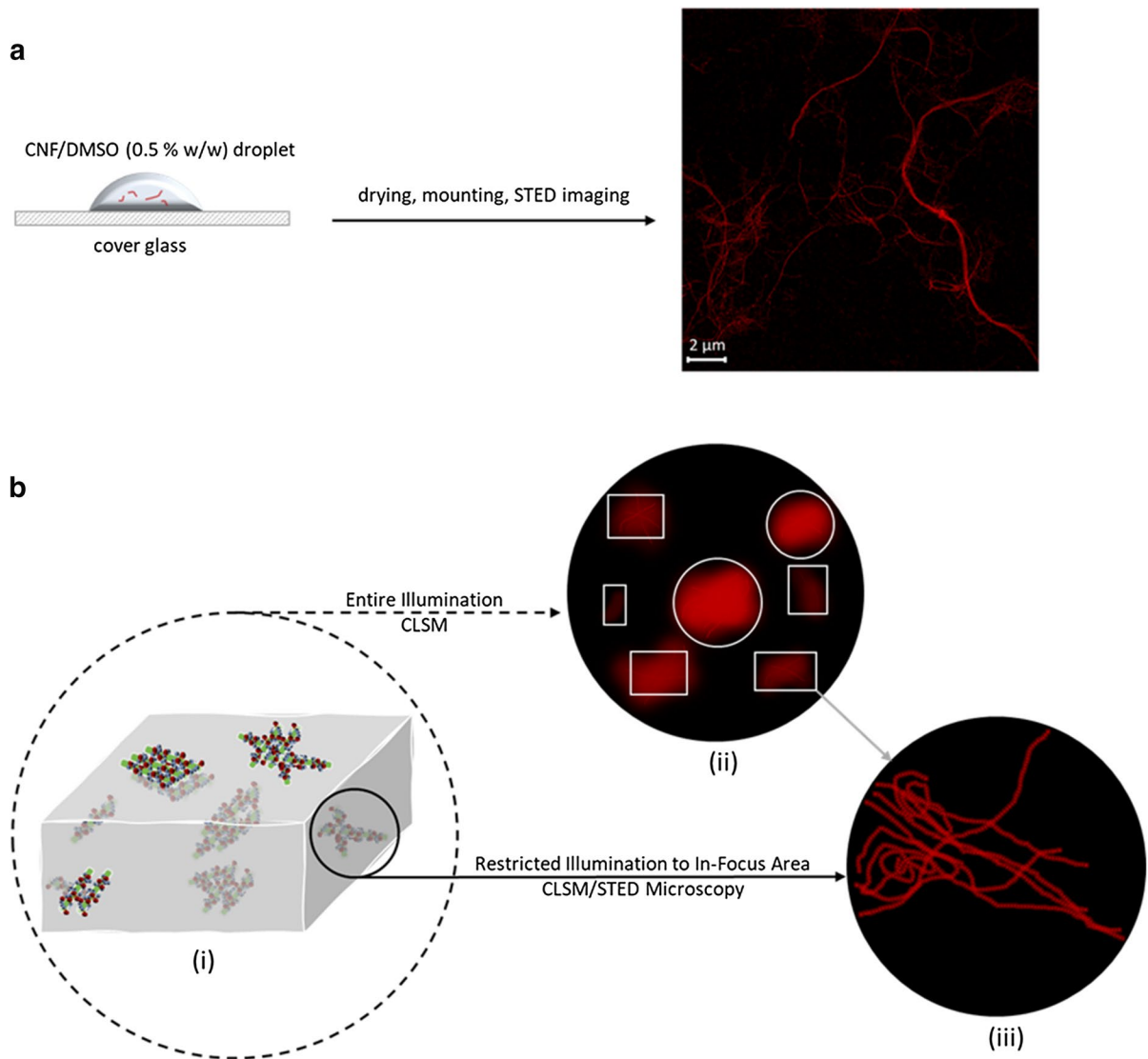


Fig. 9 Schematic illustration of **a** STED imaging of fibrils dried from DMSO, **b** Detecting distribution and morphology of modified CNFs in a PVA composite: (i) Model of modified CNFs in PVA, (ii) Concept map overview of modified CNFs in

PVA: “In-Focus” lights in circle, “Out-of-Focus” lights in rectangle, (iii) Concept image of focused modified CNF structure in PVA

in between (Fig. 7d); a cluster involves all entangled fibrils/bundles with a minimal (below 10 nm) gap (Fig. 7e).

More isolated fibrils or homogeneous networks are desired when dispersing CNFs in a solvent, e.g. DMSO, to form a stable suspension. For this, monomers with more extended hydrophilic groups, such as oligo(ethylene glycol), can be used for modifying the CNF surface, as the long hydrophilic groups interact

effectively with solvent molecules (DMSO&H₂O) and better suppress the inter-fibril interaction.

It should also be noted that for a same chromophore, the brightness of the fluorescent signals is directly proportional to the fluorophore concentration. This concentration effect can, in some cases, indicate an inhomogeneous dispersion of the CNFs, e.g. high density of dye due to large fibril aggregation. This aggregation phenomenon will lead to complete

saturation of the fluorescence signal and STED measurement can therefore not be performed.

STED and high-resolution imaging of modified CNFs in PVA

As previously introduced, the morphology of CNFs in composites is generally studied via microscopic techniques, such as AFM, SEM and TEM. A downside of these techniques is that the distinction between CNFs and the matrix (e.g. PVA) is difficult or not possible. For instance, Fig. 8a shows the surface of a modified CNF/PVA composite detected by FESEM, where the modified CNFs are fully buried. A significant

difference can be obtained by STED microscopy that modified CNFs labeled with fluorescent dyes are illuminated and revealing not only their morphology but also the spatial configuration within a PVA matrix (Fig. 8b).

We here firstly investigated the possibility to image isolated CNF nanostructure through STED microscopy. We now aimed to extend the study and see if the morphology of the modified CNFs embedded in a PVA composite could be investigated through a combination of CSLM and STED microscopy (Fig. 9). CSLM microscopy is a convenient microscopic technique, which can illuminate the entire specimen of interest and localized all the chromophores rapidly

Fig. 10 Microscopic images of modified CNFs (0.5% w/w) in PVA (10% w/w): **a** Deconvolved confocal image of cluster of AF 488&ATTO 633@ DEG-PgA-CNFs, **b**, Map overview of ATTO633@ DEG-PgA-CNFs in PVA Matrix, **c** Deconvolved STED image of cluster of ATTO633@DEG-PgA-CNFs, **d** Intrafibrillar network, **e** Single fibrills from a bundle

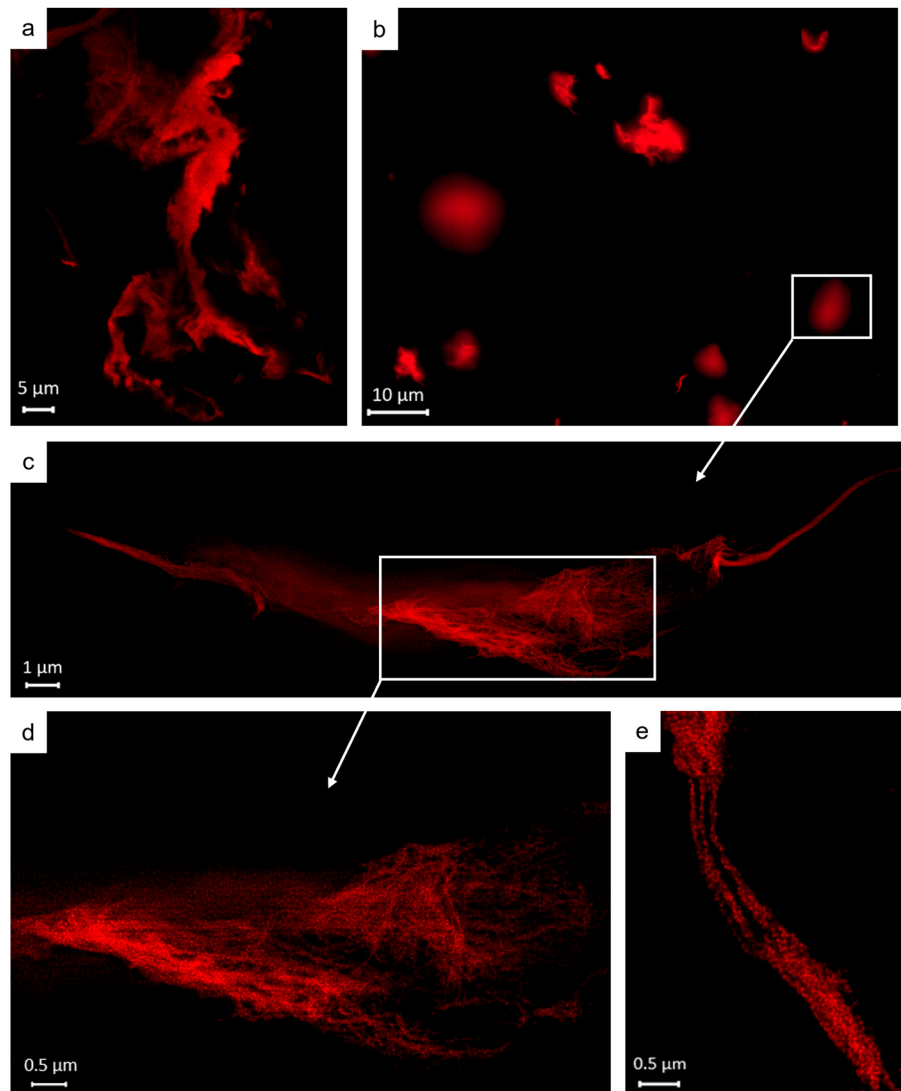
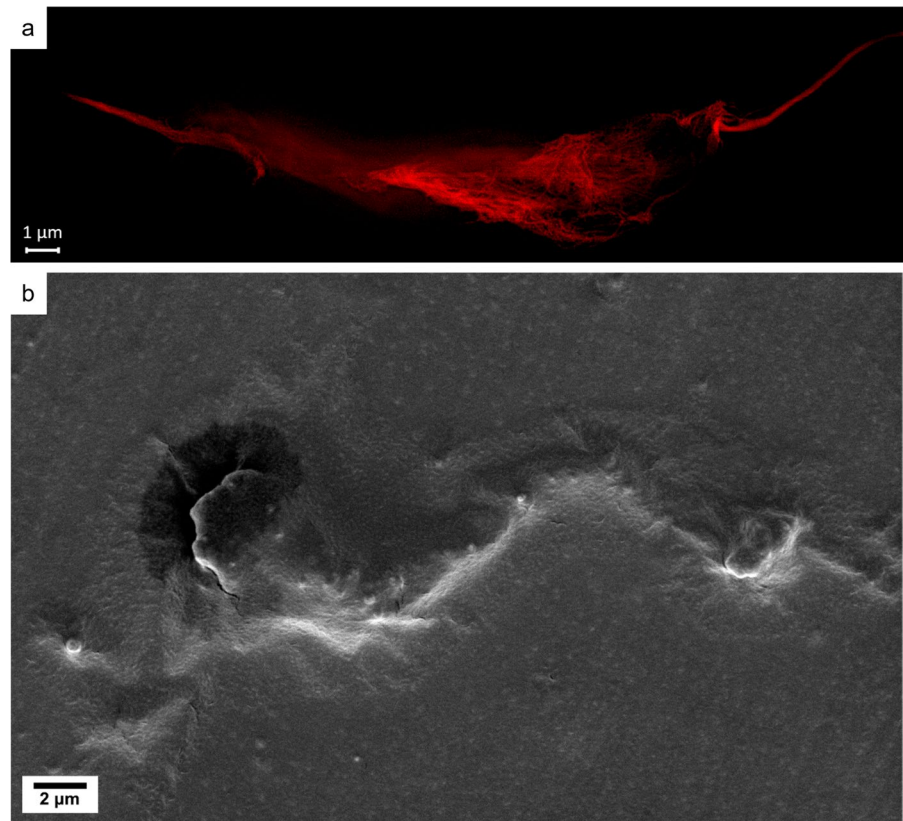


Fig. 11 ATTO633@DEG-PgA-CNFs in a PVA matrix: **a** STED image, **b** FESEM Image



at once. Combining CSLM and STED microscopy, we were able to localize the fluorescently labeled CNFs (AF488&ATTO633@DEG-PgA-CNFs and ATTO633@DEG-PgA-CNFs) and observe their distribution in the three dimensional PVA matrix (Fig. 9b). Despite the fact that both dyes had a specific function in our materials, we rapidly found out that the behavior of those two samples was completely different when mixed with the PVA matrix, and only when mixed.

In the previous STED observation, fibrils were directly deposited on a cover glass through solvent evaporation, and all the fibrils were all on the same focal plane (Fig. 9a). But now, CNFs are distributed in a PVA matrix with a thickness of approx. 10 μm , creating a 3D environment (Fig. 9b). CNFs can either disperse or form aggregates in different locations of the PVA matrix at different heights, and therefore be either on the “in-focus” plane or be observed as blurry spots when CNFs are on a “out-of-focus” plane.

The distribution and the localization of the CNFs in the PVA matrix were firstly observed with the CSLM microscope, so a large overview could be created (Fig. 10a, b). As mentioned previously, both dyes had a specific function in our materials, but their behavior was completely different when mixed with the PVA matrix. In Fig. 10a, the AF488&ATTO633@DEG-PgA-CNF show only large aggregates (between 50–100 μm). Those aggregates could not be studied by STED as the density of chromophore was too substantial, creating a complete saturation of the signal.

Interestingly for the other sample, ATTO633@DEG-PgA-CNFs, much smaller aggregates could be first observed with the CSLM (Fig. 10b). However, when those fibrils were studied with the STED, clear inter-fibrillar structures, fibril networks were observed, with a distinct distance between each fibril.

More detailed structures inside the aggregates of ATTO633@DEG-PgA-CNFs were revealed (Fig. 10c–e). Fibrils still formed a relatively

homogeneous network with a distance of max. 0.2 μm in between; fibril bundles are associated tightly in PVA.

Through STED microscopy, the modified CNFs embedded in a PVA composite are finally exposed. Now we can extrapolate fibrils detected by FESEM. Figure 11b show a classic grey-scale image obtained by FESEM, which shows an aggregate of ATTO633@DEG-PgA-CNFs on the outer face of a PVA matrix, while the deeper structure remains buried. To sum up, STED microscopy manifests its remarkable performance for the fibril morphology study.

Conclusions

We have devised a tunable strategy to surface modify CNFs via a combination of Cu^0 -mediated radical polymerization and Cu^I -catalyzed alkyne-azide cycloaddition. The spectra of ATR-IR and solid-state ^{13}C -NMR demonstrated that CNF-based macroinitiators were synthesized and initiated the growth of statistical copolymers on CNF surfaces via SET-LRP. Furthermore, the effectivity of induced terminal alkyne groups was proven by the restored fluorescence of 3-azido-7-hydroxycoumarin via click chemistry. This versatile strategy could be adapted to modify CNFs with desired properties for applications in a broad scope.

The novelty of our work lies in the morphology study of modified CNFs investigated through laser scanning microscopy and STED microscopy. With these techniques, modified CNFs embedded in a PVA composite were also detected and visualized nondestructively.

In deconvolved STED images, we found out that the grafted polymer chains wrapped around CNFs and thus the dimension of CNFs were outlined. We measured over 30 specimens with widths ranging from 56 to 68 nm and lengths of several micrometers, which match the typical dimension gained by mechanical treatment CNF production. The present study has explored the behaviors of CNFs dried from DMSO, including single fibrils, fibril networks, fibril bundles and clusters. The behavior of CNFs in a DMSO suspension needs to be explored further.

The distribution and morphology of modified CNFs embedded in a PVA composite with a thickness

of approx. 10 μm were revealed through a widefield microscope and CLSM/STED microscopes.

Acknowledgments We thank T. Potsch and Dr. A. Olbrich the Thünen Institute of Wood Research for FESEM imaging. We acknowledge Dr. P. Hernandez-Varas from the Core Facility for Integrated Microscopy, Faculty of Health and Medical Sciences, University of Copenhagen for STED imaging service.

Author contributions All authors: XJ, BM, JN contributed to the study conception and the design of the experiments. The synthesis and materials preparations were performed by XJ. The data collection and analysis were performed by XJ, BM, JN. All authors: XJ, BM, JN contributed to write the first manuscript draft and the submitted version. Participants or animals performed by any of the authors.

Funding Open Access funding enabled and organized by Projekt DEAL. J. Navarro, and all authors thank Fachagentur Nachwachsende Rohstoffe e.V. (FNR/BMEL, Project Holz-Mat3D, number 2220HV024X), for financial support.

Data availability The authors declare that the data supporting the findings of this study are available within the article.

Declarations

Conflict of interest The authors declare no competing financial interests.

Consent for publication All authors agreed with the paper content and all gave explicit consent to submit the paper to Cellulose. Moreover, we obtained consent from the responsible authorities at the institute of wood science where the work has been carried out, before the paper was submitted.

Ethical standard The authors certify that this manuscript is original and has not been published elsewhere and will not be submitted for publication in another journal while being considered by Cellulose. Moreover, this study is not split up into several parts to increase the quantity of submissions and submitted to several journals. This article does not contain any studies with human and/or Animals.

Open Access This article is licensed under a Creative Commons Attribution 4.0 International License, which permits use, sharing, adaptation, distribution and reproduction in any medium or format, as long as you give appropriate credit to the original author(s) and the source, provide a link to the Creative Commons licence, and indicate if changes were made. The images or other third party material in this article are included in the article's Creative Commons licence, unless indicated otherwise in a credit line to the material. If material is not included in the article's Creative Commons licence and your intended use is not permitted by statutory regulation or exceeds the permitted use, you will need to obtain permission directly from the copyright holder. To view a copy of this licence, visit <http://creativecommons.org/licenses/by/4.0/>.

References

- Aïssa K, Karaaslan MA, Renneckar S, Saddler JN (2019) Functionalizing cellulose nanocrystals with click modifiable carbohydrate-binding modules. *Biomacromol* 20:3087–3093. <https://doi.org/10.1021/acs.biomac.9b00646>
- Akeroyd N, Klumperman B (2011) The combination of living radical polymerization and click chemistry for the synthesis of advanced macromolecular architectures. *Eur Polym J* 47:1207–1231. <https://doi.org/10.1016/j.eurpolymj.2011.02.003>
- Anastasaki A, Nikolaou V, Simula A et al (2014) Expanding the scope of the photoinduced living radical polymerization of acrylates in the presence of CuBr₂ and Me6-Tren. *Macromolecules* 47:3852–3859. <https://doi.org/10.1021/ma500787d>
- Arof AK, Mat Nor NA, Aziz N et al (2019) Investigation on morphology of composite poly(ethylene oxide)cellulose nanofibers. *Mater Today Proc* 17:388–393. <https://doi.org/10.1016/j.matpr.2019.06.265>
- Babi M, Fatona A, Li X et al (2022) Efficient labeling of nanocellulose for high-resolution fluorescence Microscopy applications. *Biomacromol* 23:1981–1994. <https://doi.org/10.1021/acs.biomac.1c01698>
- Bao C, Yin Y, Zhang Q (2018) Synthesis and assembly of laccase-polymer giant amphiphiles by self-catalyzed CuAAC click chemistry. *Biomacromol* 19:1539–1551. <https://doi.org/10.1021/acs.biomac.8b00087>
- Beaumont M, Bacher M, Opietnik M et al (2018) A general aqueous silanization protocol to introduce vinyl, mercapto or azido functionalities onto cellulose fibers and nanocelluloses. *Molecules* 23:1427. <https://doi.org/10.3390/molecules23061427>
- Busko D, Balushev S, Crespy D et al (2012) New possibilities for materials science with STED microscopy. *Micron* 43:583–588. <https://doi.org/10.1016/j.micron.2011.10.003>
- Calovi S, Soria FN, Tønnesen J (2021) Super-resolution STED microscopy in live brain tissue. *Neurobiol Dis* 156:105420. <https://doi.org/10.1016/j.nbd.2021.105420>
- Chiefari J, Chong(Bill) YK, Ercole F, Krstina J, Jeffery J, Le TP, Mayadunne RTA, Meijs GF, Moad CL, Moad G, Rizzardo E, Thang SH (1998) Living free-radical polymerization by reversible addition–fragmentation chain transfer: the RAFT process. *Macromolecules* 31(16):5559–5562. <https://doi.org/10.1021/ma9804951>
- Edwards JV, Prevost N, Sethumadhavan K et al (2013) Peptide conjugated cellulose nanocrystals with sensitive human neutrophil elastase sensor activity. *Cellulose* 20:1223–1235. <https://doi.org/10.1007/s10570-013-9901-y>
- Fazeli M, Keley M, Biazar E (2018) Preparation and characterization of starch-based composite films reinforced by cellulose nanofibers. *Int J Biol Macromol* 116:272–280. <https://doi.org/10.1016/j.ijbiomac.2018.04.186>
- Fleischmann S, Percec V (2010) SET-LRP of methyl methacrylate initiated with CCl₄ in the presence and absence of air. *J Polym Sci Part A Polym Chem* 48:2243–2250. <https://doi.org/10.1002/pola.24000>
- Friedemann K, Turshatov A, Landfester K, Crespy D (2011) Characterization via two-color STED microscopy of nanostructured materials synthesized by colloid electrospinning. *Langmuir* 27:7132–7139. <https://doi.org/10.1021/la104817r>
- Frome AN, Berlioz S, Chailan JF, Panaitescu DM (2013) Morphology and thermal properties of PLA-cellulose nanofibers composites. *Carbohydr Polym* 91:377–384. <https://doi.org/10.1016/j.carbpol.2012.08.054>
- Fukuzumi H, Tanaka R, Saito T, Isogai A (2014) Dispersion stability and aggregation behavior of TEMPO-oxidized cellulose nanofibrils in water as a function of salt addition. *Cellulose* 21:1553–1559. <https://doi.org/10.1007/s10570-014-0180-z>
- Gårdebjer S, Bergstrand A, Idström A et al (2015) Solid-state NMR to quantify surface coverage and chain length of lactic acid modified cellulose nanocrystals, used as fillers in biodegradable composites. *Compos Sci Technol* 107:1–9. <https://doi.org/10.1016/j.compscitech.2014.11.014>
- Georgouvelas D, Jalvo B, Valencia L et al (2020) Residual lignin and zwitterionic polymer grafts on cellulose nanocrystals for antifouling and antibacterial applications. *ACS Appl Polym Mater* 2:3060–3071. <https://doi.org/10.1021/acsapm.0c00212>
- Golmohammadi H, Morales-Narváez E, Naghdi T, Merkoçi A (2017) Nanocellulose in sensing and biosensing. *Chem Mater* 29:5426–5446. <https://doi.org/10.1021/acs.chemmater.7b01170>
- Goodge K, Frey M (2020) Biotin-conjugated cellulose nanofibers prepared via copper-catalyzed alkyne-azide cycloaddition (CuAAC) “click” chemistry. *Nanomaterials* 10:1172. <https://doi.org/10.3390/nano10061172>
- Guise, C., & Figueiro, R. (2016). Biomedical applications of nanocellulose. In natural fibres: advances in science and technology towards industrial applications. Springer, Dordrecht, pp (155–169)
- Gustavsson LH, Adolffson KH, Hakkarainen M (2020) Thermoplastic “all-cellulose” composites with covalently attached carbonized cellulose. *Biomacromol* 21(5):1752–1761. <https://doi.org/10.1021/acs.biomac.9b01672>
- Hein JE, Fokin VV (2010) Copper-catalyzed azide-alkyne cycloaddition (CuAAC) and beyond: new reactivity of copper(i) acetylides. *Chem Soc Rev* 39:1302–1315. <https://doi.org/10.1039/b904091a>
- Hettegger H, Beaumont M, Potthast A, Rosenau T (2016) Aqueous modification of nano- and microfibrillar cellulose with a click synthon. *Chemsuschem* 9:75–79. <https://doi.org/10.1002/cssc.201501358>
- Himo F, Lovell T, Hilgraf R et al (2005) Copper(I)-catalyzed synthesis of azoles. DFT study predicts unprecedented reactivity and intermediates. *J Am Chem Soc* 127:210–216. <https://doi.org/10.1021/ja0471525>
- Huang B, Babcock H, Zhuang X (2010) Breaking the diffraction barrier: super-resolution imaging of cells. *Cell* 143:1047–1058. <https://doi.org/10.1016/j.cell.2010.12.002>
- Hur J, Park S, Kim JH et al (2022) ultrasensitive, transparent, flexible, and ecofriendly NO₂ gas sensors enabled by oxidized single-walled carbon nanotube bundles on cellulose with engineered surface roughness. *ACS Sustain Chem Eng* 10:3227–3235. <https://doi.org/10.1021/acssuschemeng.1c07559>

- Inglis AJ, Sinnwell S, Stenzel MH, Barner-Kowollik C (2009) Ultrafast click conjugation of macromolecular building blocks at ambient temperature. *Angew Chemie - Int Ed* 48:2411–2414. <https://doi.org/10.1002/anie.200805993>
- Junka K, Filpponen I, Johansson L-S et al (2014) A method for the heterogeneous modification of nanofibrillar cellulose in aqueous media. *Carbohydr Polym* 100:107–115. <https://doi.org/10.1016/j.carbpol.2012.11.063>
- Kalia S, Boufi S, Celli A, Kango S (2014) Nanofibrillated cellulose: surface modification and potential applications. *Colloid Polym Sci* 292:5–31. <https://doi.org/10.1007/s00396-013-3112-9>
- Kaur J, Saxena M, Rishi N (2021) An overview of recent advances in biomedical applications of click chemistry. *Bioconjug Chem* 32:1455–1471. <https://doi.org/10.1021/acs.bioconjchem.1c00247>
- Kelly PV, Cheng P, Gardner DJ, Gramlich WM (2021) Aqueous polymer modification of cellulose nanofibrils by grafting-through a reactive methacrylate group. *Macromol Rapid Commun* 42:2000531. <https://doi.org/10.1002/marc.202000531>
- Klemm D, Kramer F, Moritz S et al (2011) Nanocelluloses: a new family of nature-based materials. *Angew Chemie Int Ed* 50:5438–5466. <https://doi.org/10.1002/anie.201001273>
- Kloetzel MC (2011) The diels-alder reaction with maleic anhydride. *Org. React.* 1–59
- Lalanne-Tisné M, Mees MA, Eyley S et al (2020) Organocatalyzed ring opening polymerization of lactide from the surface of cellulose nanofibrils. *Carbohydr Polym* 250:1–22. <https://doi.org/10.1016/j.carbpol.2020.116974>
- Larsson E, Sanchez CC, Porsch C et al (2013) Thermo-responsive nanofibrillated cellulose by polyelectrolyte adsorption. *Eur Polym J* 49:2689–2696. <https://doi.org/10.1016/j.eurpolymj.2013.05.023>
- Lee KY, Blaker JJ, Murakami R et al (2014) Phase behavior of medium and high internal phase water-in-oil emulsions stabilized solely by hydrophobized bacterial cellulose nanofibrils. *Langmuir* 30:452–460. <https://doi.org/10.1021/la4032514>
- Levere ME, Nguyen NH, Leng X, Percec V (2013) Visualization of the crucial step in SET-LRP. *Polym Chem* 4:1635–1647. <https://doi.org/10.1039/C2PY21084C>
- Liimatainen H, Visanko M, Sirviö JA et al (2012) Enhancement of the nanofibrillation of wood cellulose through sequential periodate-chlorite oxidation. *Biomacromol* 13:1592–1597. <https://doi.org/10.1021/bm300319m>
- Liu Y, Peng Z, Peng X et al (2021) Shedding new lights into STED microscopy: emerging nanoprobes for imaging. *Front Chem* 9:1–22. <https://doi.org/10.3389/fchem.2021.641330>
- Lizundia E, Meario E, Vilas JL (2016) Grafting of cellulose nanocrystals. In: multifunctional polymeric nanocomposites based on cellulosic reinforcements. Elsevier, 61–113
- Majoinen J, Walther A, McKee JR et al (2011) Polyelectrolyte brushes grafted from cellulose nanocrystals Using Cu-mediated surface-initiated controlled radical polymerization. *Biomacromol* 12:2997–3006. <https://doi.org/10.1021/bm200613y>
- Malkoch M, Thibault RJ, Drockenmuller E et al (2005) Orthogonal approaches to the simultaneous and cascade functionalization of macromolecules using click chemistry. *J Am Chem Soc* 127:14942–14949. <https://doi.org/10.1021/ja0549751>
- Mietner JB, Jiang X, Edlund U et al (2021) 3D printing of a bio-based ink made of cross-linked cellulose nanofibrils with various metal cations. *Sci Rep* 11:1–9. <https://doi.org/10.1038/s41598-021-85865-4>
- Moon RJ, Martini A, Nairn J et al (2011) Cellulose nanomaterials review: structure, properties and nanocomposites. *Chem Soc Rev* 40:3941. <https://doi.org/10.1039/c0cs00108b>
- Nakagaito AN, Yano H (2004) The effect of morphological changes from pulp fiber towards nano-scale fibrillated cellulose on the mechanical properties of high-strength plant fiber based composites. *Appl Phys A Mater Sci Process* 78:547–552. <https://doi.org/10.1007/s00339-003-2453-5>
- Navarro JRG, Edlund U (2017) Surface-initiated controlled radical polymerization approach to enhance nanocomposite integration of cellulose nanofibrils. *Biomacromol* 18:1947–1955. <https://doi.org/10.1021/acs.biomac.7b00398>
- Navarro JRG, Conzatti G, Yu Y et al (2015) Multicolor fluorescent labeling of cellulose nanofibrils by click chemistry. *Biomacromol* 16:1293–1300. <https://doi.org/10.1021/acs.biomac.5b00083>
- Navarro JRG, Rostami J, Ahlinder A et al (2020) Surface-initiated controlled radical polymerization approach to in situ cross-link cellulose nanofibrils with inorganic nanoparticles. *Biomacromol* 21:1952–1961. <https://doi.org/10.1021/acs.biomac.0c00210>
- Nguyen NH, Rosen BM, Percec V (2010) SET-LRP of N, N-dimethylacrylamide and of N-isopropylacrylamide at 25 °C in protic and in dipolar aprotic solvents. *J Polym Sci Part A Polym Chem* 48:1752–1763. <https://doi.org/10.1002/pola.23940>
- Nguyen NH, Levere ME, Percec V (2012) SET-LRP of methyl acrylate to complete conversion with zero termination. *J Polym Sci Part A Polym Chem* 50:860–873. <https://doi.org/10.1002/pola.25838>
- Nguyen NH, Kulis J, Sun H-J et al (2013) A comparative study of the SET-LRP of oligo(ethylene oxide) methyl ether acrylate in DMSO and in H₂O. *Polym Chem* 4:144–155. <https://doi.org/10.1039/C2PY20782F>
- Nicol E, Derouineau T, Puaud F, Zaitsev A (2012) Synthesis of double hydrophilic poly(ethylene oxide)-b-poly(2-hydroxyethyl acrylate) by single-electron transfer-living radical polymerization. *J Polym Sci Part A Polym Chem* 50:3885–3894. <https://doi.org/10.1002/pola.26185>
- Nilsson C, Simpson N, Malkoch M et al (2008) Synthesis and thiol-ene photopolymerization of allyl-ether functionalized dendrimers. *J Polym Sci Part A Polym Chem* 46:1339–1348. <https://doi.org/10.1002/pola.22474>
- Ning L, You C, Zhang Y et al (2021) Polydopamine loaded fluorescent nanocellulose–agarose hydrogel: a pH-responsive drug delivery carrier for cancer therapy. *Compos Commun* 26:100739. <https://doi.org/10.1016/j.coco.2021.100739>
- Nogi M, Abe K, Handa K et al (2006) Property enhancement of optically transparent bionanofiber composites by acetylation. *Appl Phys Lett* 89:233123. <https://doi.org/10.1063/1.2403901>

- Ottenhall A, Illergård J, Ek M (2017) Water purification using functionalized cellulose fibers with nonleaching bacteria adsorbing properties. *Environ Sci Technol* 51:7616–7623. <https://doi.org/10.1021/acs.est.7b01153>
- Percec V, Guliashvili T, Ladislav JS et al (2006) Ultrafast synthesis of ultrahigh molar mass polymers by metal-catalyzed living radical polymerization of acrylates, methacrylates, and vinyl chloride mediated by SET at 25 °C. *J Am Chem Soc* 128:14156–14165. <https://doi.org/10.1021/ja065484z>
- Poonguzhali R, Khaleel Basha S, Sugantha Kumari V (2018) Novel asymmetric chitosan/PVP/nanocellulose wound dressing: in vitro and in vivo evaluation. *Int J Biol Macromol* 112:1300–1309. <https://doi.org/10.1016/j.ijbiomac.2018.02.073>
- Presolski SI, Hong VP, Finn MG (2011) Copper-catalyzed azide-alkyne click chemistry for bioconjugation. *Curr Protoc Chem Biol* 3:153–162. <https://doi.org/10.1002/9780470559277.ch110148>
- Radakisinin R, Abdul Majid MS, Jamir MRM et al (2020) Structural, morphological and thermal properties of cellulose nanofibers from napier fiber (*Pennisetum purpureum*). *Materials (basel)* 13:4125. <https://doi.org/10.3390/ma13184125>
- Ramapanicker R, Chauhan P (2016) Click chemistry: mechanistic and synthetic perspectives. *Click React Org Synth*. <https://doi.org/10.1002/9783527694174.ch1>
- Roobala C, Ilanila IP, Basu JK (2018) Applications of STED fluorescence nanoscopy in unravelling nanoscale structure and dynamics of biological systems. *J Biosci* 43:471–484. <https://doi.org/10.1007/s12038-018-9764-3>
- Rosen BM, Percec V (2009) Single-electron transfer and single-electron transfer degenerative chain transfer living radical polymerization. *Chem Rev* 109:5069–5119. <https://doi.org/10.1021/cr900024j>
- Saba N, Mohammad F, Pervaiz M et al (2017) Mechanical, morphological and structural properties of cellulose nanofibers reinforced epoxy composites. *Int J Biol Macromol* 97:190–200. <https://doi.org/10.1016/j.ijbiomac.2017.01.029>
- Salari M, Bitounis D, Bhattacharya K et al (2019) Development & characterization of fluorescently tagged nanocellulose for nanotoxicological studies. *Environ Sci Nano* 6:1516–1526. <https://doi.org/10.1039/c8en01381k>
- Samanta SR, Levere ME, Percec V (2013) SET-LRP of hydrophobic and hydrophilic acrylates in trifluoroethanol. *Polym Chem* 4:3212–3224. <https://doi.org/10.1039/c3py00289f>
- Samanta SR, Nikolaou V, Keller S et al (2015) Aqueous SET-LRP catalyzed with “in situ” generated Cu(0) demonstrates surface mediated activation and bimolecular termination. *Polym Chem* 6:2084–2097. <https://doi.org/10.1039/C4PY01748J>
- Schermelleh L, Heintzmann R, Leonhardt H (2010) A guide to super-resolution fluorescence microscopy. *J Cell Biol* 190:165–175. <https://doi.org/10.1083/jcb.201002018>
- Schyrer B, Pasche S, Voirin G et al (2014) Biosensors based on porous cellulose nanocrystal-poly(vinyl alcohol) scaffolds. *ACS Appl Mater Interfaces* 6:12674–12683. <https://doi.org/10.1021/am502670u>
- Sezgin E, Schneider F, Galiani S et al (2019) Measuring nanoscale diffusion dynamics in cellular membranes with super-resolution STED-FCS. *Nat Protoc* 14:1054–1083. <https://doi.org/10.1038/s41596-019-0127-9>
- Sivakumar K, Xie F, Cash BM et al (2004) A fluorogenic 1,3-dipolar cycloaddition reaction of 3-azidocoumarins and acetylenes. *Org Lett* 6:4603–4606. <https://doi.org/10.1021/ol047955x>
- Song W, Xiao C, Cui L et al (2012) Facile construction of functional biosurface via SI-ATRP and “click glycosylation.” *Colloids Surf B Biointerfaces* 93:188–194. <https://doi.org/10.1016/j.colsurfb.2012.01.002>
- Stephan T, Roesch A, Riedel D, Jakobs S (2019) Live-cell STED nanoscopy of mitochondrial cristae. *Sci Rep* 9:1–6. <https://doi.org/10.1038/s41598-019-48838-2>
- Stockhammer A, Bottanelli F (2021) Appreciating the small things in life: STED microscopy in living cells. *J Phys D Appl Phys* 54:033001. <https://doi.org/10.1088/1361-6463/abac81>
- Storms-Miller WK, Pugh C (2015) Prop-2-yn-1-yl 2-Bromo-2-methylpropanoate: identification and suppression of side reactions of a commonly used terminal alkyne-functional ATRP initiator. *Macromolecules* 48:3803–3810. <https://doi.org/10.1021/acs.macromol.5b00652>
- Tsubokawa N, Iida T, Takayama T (2000) Modification of cellulose powder surface by grafting of polymers with controlled molecular weight and narrow molecular weight distribution. *J Appl Polym Sci* 75:515–522. [https://doi.org/10.1002/\(SICI\)1097-4628\(20000124\)75:4%3c515::AID-APP6%3e3.0.CO;2-Q](https://doi.org/10.1002/(SICI)1097-4628(20000124)75:4%3c515::AID-APP6%3e3.0.CO;2-Q)
- Urban NT, Willig KI, Hell SW, Nägerl UV (2011) STED nanoscopy of actin dynamics in synapses deep inside living brain slices. *Biophys J* 101:1277–1284. <https://doi.org/10.1016/j.bpj.2011.07.027>
- Vicidomini G, Bianchini P, Diaspro A (2018) STED super-resolved microscopy. *Nat Methods* 15:173–182. <https://doi.org/10.1038/nmeth.4593>
- Voronova MI, Lebedeva TN, Radugin MV et al (2006) Interactions of water-DMSO mixtures with cellulose. *J Mol Liq* 126:124–129. <https://doi.org/10.1016/j.molliq.2005.12.001>
- Wang Q, Chan TR, Hilgraf R et al (2003) Bioconjugation by copper(I)-catalyzed azide-alkyne [3 + 2] cycloaddition. *J Am Chem Soc* 125:3192–3193. <https://doi.org/10.1021/ja021381e>
- Wang K, Li W, Gao C (2007) Poly(ϵ -caprolactone)-functionalized carbon nanofibers by surface-initiated ring-opening polymerization. *J Appl Polym Sci* 105:629–640. <https://doi.org/10.1002/app.26285>
- Willberg-Keyriläinen P, Vartiainen J, Pelto J, Ropponen J (2017) Hydrophobization and smoothing of cellulose nanofibril films by cellulose ester coatings. *Carbohydr Polym* 170:160–165. <https://doi.org/10.1016/j.carbpol.2017.04.082>
- Wu W, Song R, Xu Z et al (2018) Fluorescent cellulose nanocrystals with responsiveness to solvent polarity and ionic strength. *Sens Actuators, B Chem* 275:490–498. <https://doi.org/10.1016/j.snb.2018.07.085>
- Xhanari K, Syverud K, Chinga-Carrasco G et al (2011) Structure of nanofibrillated cellulose layers at the o/w interface.

- J Colloid Interface Sci 356:58–62. <https://doi.org/10.1016/j.jcis.2010.12.083>
- Xiong L, Zhan F, Liang H et al (2018) Chemical grafting of nano-TiO₂ onto carbon fiber via thiol–ene click chemistry and its effect on the interfacial and mechanical properties of carbon fiber/epoxy composites. *J Mater Sci* 53:2594–2603. <https://doi.org/10.1007/s10853-017-1739-5>
- Zhai S, Chen H, Zhang Y et al (2022) Nanocellulose: a promising nanomaterial for fabricating fluorescent composites. *Cellulose* 29:7011–7035. <https://doi.org/10.1007/s10570-022-04700-9>
- Zhang R, Liu Y (2018) High energy oxidation and organo-solv solubilization for high yield isolation of cellulose nanocrystals (CNC) from Eucalyptus hardwood. *Sci Rep* 8:1–11. <https://doi.org/10.1038/s41598-018-34667-2>
- Zhang N, Samanta SR, Rosen BM, Percec V (2014a) Single electron transfer in radical ion and radical-mediated organic, materials and polymer synthesis. *Chem Rev* 114:5848–5958. <https://doi.org/10.1021/cr400689s>
- Zhang Q, Wilson P, Anastasaki A et al (2014b) Synthesis and aggregation of double hydrophilic diblock glycopolymers via aqueous SET-LRP. *ACS Macro Lett* 3:491–495. <https://doi.org/10.1021/mz5001724>

Publisher's Note Springer Nature remains neutral with regard to jurisdictional claims in published maps and institutional affiliations.